7 Nusselt number distribution as a function of the flow angle in the stagnation region

7.1 Introduction

The possibility that the difference of the Nusselt number between the two-layer stagnation gauge and the single-layer one could be originated by the combination of:
a) a strong misplacement of the former gauge on the blade profile,
b) high changes in the flow incidence angle that could move significantly the stagnation point on the blade profile during a test in the turbine facility CT3,
was finally excluded by the experimental investigation described in paragraph 7.2. Further numerical investigation based on blade prediction (paragraph 7.3) investigate more into detail the influence of the stagnation point by the flow incidence. Finally, the Nusselt number distribution is numerically calculated across the blade profile in order to give a rough estimation of the expected values in the stagnation region.

7.2 Experimental determination of the stagnation gauge positions and their deviation according to variations of flow incidence angle

In the stagnation region of the blade, the thickness of the boundary layer development when the blade is submitted to a flow takes minimum values compared to the rest of the blade; while at the stagnation point, the boundary layer thickness is zero. Thus, high wall heat flux is observed in the stagnation region with its highest value at the stagnation point; more specifically, the wall heat flux distribution on the blade profile next to the stagnation point radically decreases even for small distances such as *1-2%* of the blade axial chord. The accurate knowledge of the position of the gauge in the stagnation region is of high importance, when the wall heat flux at the stagnation point has to be experimentally determined. The next series of experiments are performed in order to verify if the position of the stagnation gauges for the single-layer (211, chapter 4) and for the two-layer (511, chapter 5) gauges used for the measurements on the second stator blade in the CT3 facility are well centered at the stagnation point. The influence of the flow incidence angle on the Nusselt number measurements is also experimentally assessed using an approximation of the blade stagnation region to a cylinder.

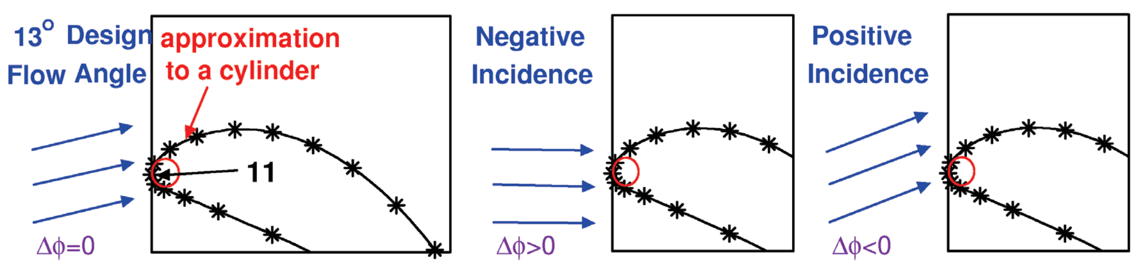

Figure 7-1: Position of the single-layer gauges on the blade profile of the second stator of CT3 (stars) and approximation of the leading edge by a cylinder

The stagnation point where the gauge 11 for the single and the two-layer array of gauges is supposed to be placed can be approximated by a cylinder (Table 6-1); the radius of this cylinder is inversely proportional to the curvature of the blade at the stagnation point (see Figure 7-1, and Figure 6-2). The same kind of experiments as for the calibration described in paragraph 3.9.4 are used in order to reproduce a constant Nusselt number depending on the incidence angle of the air jet flow ($\Delta\Phi$). The design value of the flow angle during the blade operation in the CT3 facility (chapters 4 and 5) is *13°* from the axial direction of the facility (see Figure 7-1). Thus, this design value is taken as reference for the following analysis (see Figure 7-4) and is indicated as $\Delta\Phi=0°$. Positive $\Delta\Phi$ stands for negative incidence angle, so the stagnation point moves further to the suction side of the blade. In reality, the entire cassette is rotated (see Figure 7-2). Note that the position of the stagnation gauge 11 with respect to the jet exit location does not change during the rotation of the cassette. The positive and negative rotation is also indicated at the bottom of the figure. The cassette consists of three blades, the inside and the outside casing. The Upilex sheet together with the two-layer array of gauges is glued on the central blade. There is also a second cassette with ceramic inserts that are instrumented with single-layer gauges. The insert that includes the single-layer gauge 11 is positioned on the first blade of the cassette. In Figure 7-2, the black shutter and the red reservoir are also shown. The exit of the nozzle is completely covered by the shutter.

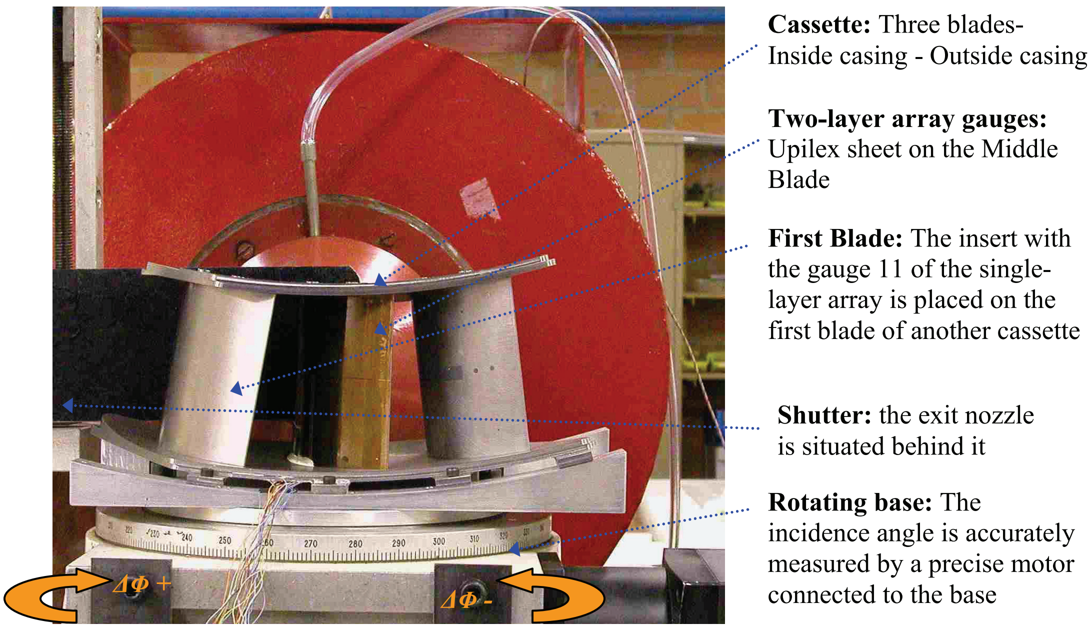

Figure 7-2: Experimental set up

The wall temperature history for the two-layer gauge (black line) and for the single-layer one (red line) is shown in Figure 7-3, on the left. The corresponding wall heat flux as a function of the wall temperature is shown on the right of the Figure 7-3, for both cases. The measurements are made at almost the same gas conditions for both gauges and at a zero $\Delta\Phi$. The gas temperature is around *360 K* and the gas total pressure difference to the atmospheric one is no more than *2.5 kPa* after the shutter opens and once the flow is established (top left graph of Figure 3-11). Please, notice that the time where the values of the wall heat flux and the temperature are used for the Nusselt number determination is shortly after the flow establishment and it does not exceed one second after the shutter opening. Thus, the flow can be considered steady as far as the Reynolds number and the wall Nusselt number are concerned, while the one dimensionality of the substrate conduction can also be ensured. This time is indicated as data reduction time on both graphs of Figure 7-3. Also, during this time, the two wall temperatures and the two heat fluxes for the two-layer and the single-layer gauges are quite close.

The Nusselt number distribution as a function of the flow angle on the single-layer gauge 11 is shown at the left side of Figure 7-4, for two series of Reynolds number. Nusselt number and Reynolds number are based on the diameter of the approximated cylinder, equal to *2x1.749mm* (Table 6-1). A plateau of Nusselt number is observed between *–20* till *+20°*. Then for both sides, the Nusselt number starts to drop as the flow angle increases. There are no measurements below –*23°*, because of the limited turning of the cassette allowed by the proximity of the shutter (see Figure 7-2).

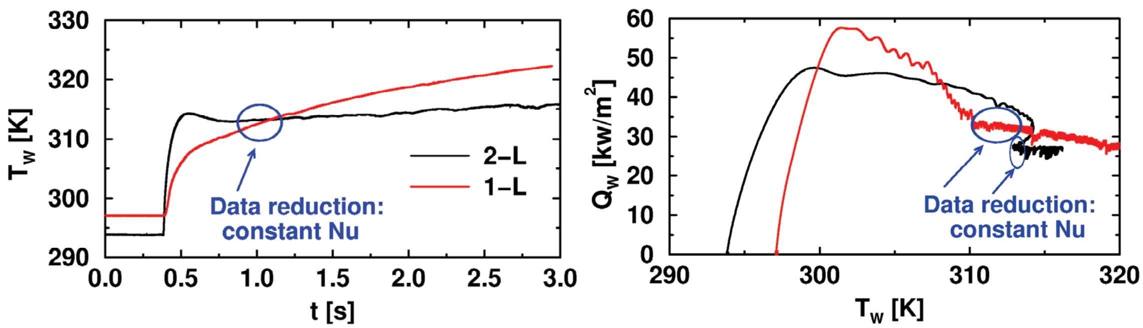

Figure 7-3: Wall temperature history (left) and wall heat flux as a function of wall temperature (right) for the two-layer gauge (in black) and for the single-layer one (in red)

The same analysis is performed for the two-layer gauge indicated on the right side of Figure 7-4. Although at zero *ΔΦ*, the Nusselt number values are the same than those calculated for the single-layer gauge, *6%* higher values are observed at angles between *–15°* and *–5°*, for both series of Reynolds number. These higher values could be eventually initiated by an error in the absolute value of the wall temperature, T_W, of the blade. Note that the temperature difference (T_{GAS} -T_W) for the Nusselt number calculations is small, of the order of *50 K*, and as a result half a Kelvin of error on the wall temperature can generate *1%* error on the Nusselt number calculations. In order to visualize the above comparison, red dotted lines have been added on the figure that correspond to the average Nusselt number values of the single-layer gauges.

The most interesting observation is that the Nusselt number plateau is limited between –*15°* and *0°* for the two-layer gauge. Then, the Nusselt number is decreasing symmetrically fom further angles of turning. Thus, the two-layer gauge 11 is probably not placed exactly at the stagnation point, but slightly further to the pressure side of the blade profile. An incidence *ΔΦ* of *10°* corresponds to a misplacement of the gauge at the stagnation point of *0.31 mm* (*2x1.749mm x 3.14 x 10/360*). Note that the single-layer gauges are painted on the Macor blade and as a result their position is likely to be exactly at the required one, contrary to the two-layer gauges placed on the Upilex-S sheet that is glued on the blade.

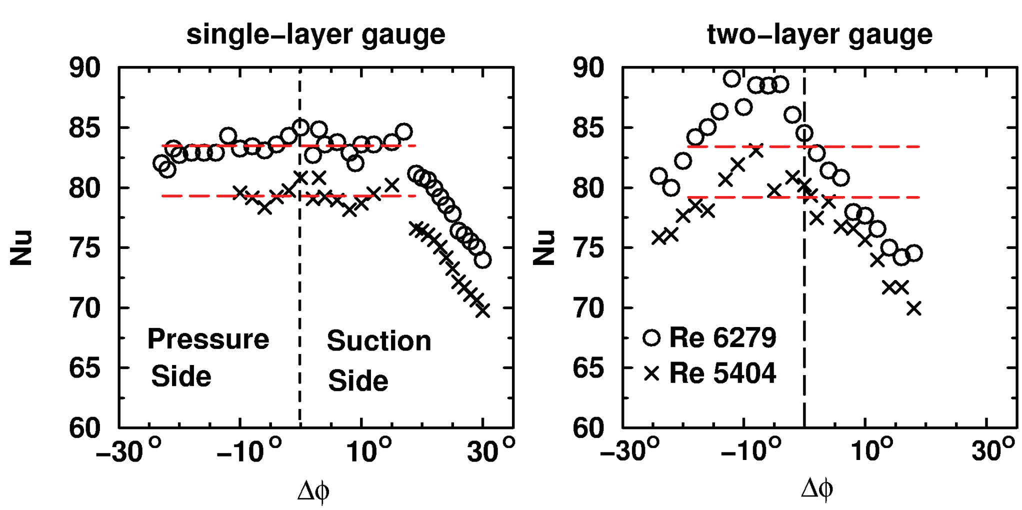

Figure 7-4: Nusselt number distribution as a function of the flow angle on the gauge 11 for the single-layer (left) and the two-layer (right) gauges

Another difference between the two measurement techniques is that the Nusselt number plateau measured with the two-layer gauge is much smaller compared to the one measured with the single-layer gauge. The latter indicates that the Upilex sheet, while being glued on the metallic blade, was more pointed at the stagnation region than the blade itself. The overcoming of the difficulty of gluing a flat surface (Upilex sheet) on a rounded one (blade) mainly depends on the capability of the assembler.

Heat transfer measurements were performed for cylinders placed in cross flow at three nominal values of Reynolds number ($7.5 \cdot 10^4$, 10^5, $1.25 \cdot 10^5$, shown in black, red and blue respectively in Figure 7-5) as well as varying levels of turbulence intensity (indicated with different symbols on the Reynolds number lines) by Kestin and Wood (1971). The data for the stagnation line can all be correlated against the single parameter $Nu/Re^{1/2}$ (see Eq. (43)). Also, all the data are plotted with one colour for each Reynolds number and one type of line for each free stream turbulence intensity in Figure 7-5 for different flow incidence angles, $\Delta\Phi$. On the same graph, the data obtained with the single-layer gauge 11 (data from Figure 7-4) for both Reynolds number levels are superimposed (indicated as stars). Note that the ratio $Nu/Re^{1/2}$ is influenced by two parameters, both Reynolds number and Turbulence intensity:

$$\frac{Nu}{Re^{1/2}} = 0.945 + 3.48\left(\frac{TuRe^{1/2}}{100}\right) - 3.99\left(\frac{TuRe^{1/2}}{100}\right)^2 . \tag{43}$$

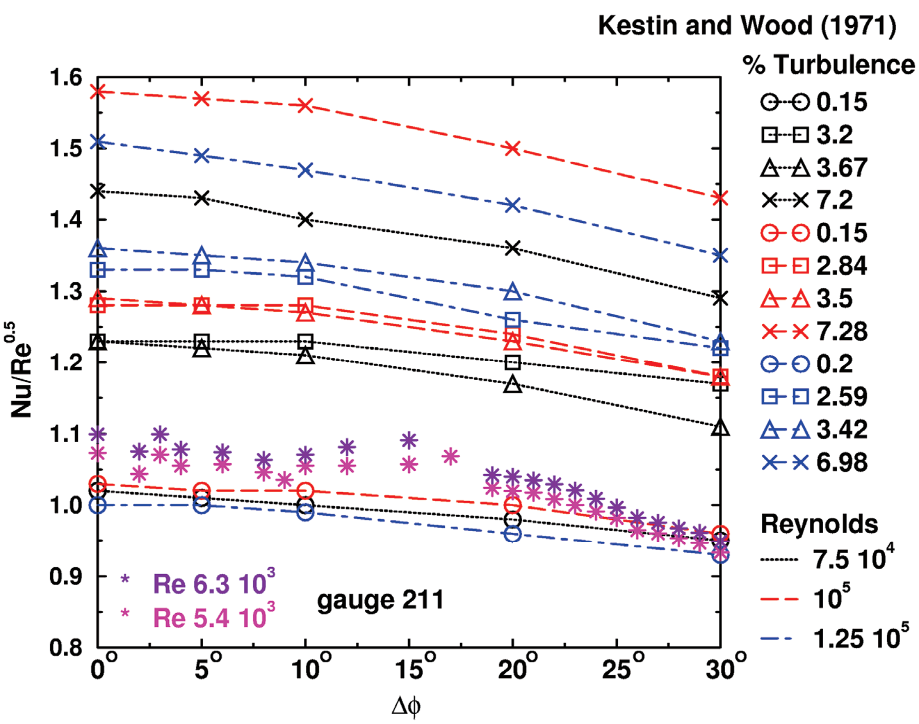

Figure 7-5: Correlation between Nusselt number, Reynolds number and Turbulence intensity around the stagnation line of a cylinder for different flow incidence angles (Kestin and Wood, 1971)

According to Eq. (43), the first series of Reynolds number ($6.3 \cdot 10^3$) is performed at around *4%* turbulence and the second series of Reynolds number ($5.4 \cdot 10^3$) is performed at around *5.1%*. The actual free stream turbulence intensity was not measured for these series of experiments. However, it was found *0.8%* inside the potential core of the flow at the exit of another nozzle used for the two-layer gauges calibration (paragraph 3.9.1) and reached values of *6-7%* outside the core. The high numbers of the calculated turbulence intensity for the measurements of Figure 7-4 could not result from the fact that the gauge is only partially in the core of the jet, where the turbulence intensity is much higher. Note that the blade is not far from the exit of the nozzle (approximately one and a half nozzle diameter). Apparently, the application of Eq. (43) for Reynolds numbers of one order of magnitude smaller than the experiments of Kestin and Wood should be avoided.

It should be pointed out that these series of measurements were performed on the blade whose stagnation region was approximated to a cylinder and compared to measurements on real cylinders. A $\Delta\Phi$ of ±*30°* corresponds to *0.92 mm* (*2x1.749mm x 3.14 x 30/360*) left and right to the stagnation point of the blade profile. This distance can not be considered negligible at this region of the blade, where the curvature gradient is very high (especially at the pressure side) compared to the rest of the blade profile. Thus, as far as the single-layer gauge is concerned, the approximation of its stagnation region with a cylinder should rather be accepted between *0°* and ±*15°*, where the Nusselt number seems to stay constant (Figure 7-4); while for the two-layer gauge, the constant Nusselt number region is much smaller.

An attempt to generalize the conclusion that the value of Nusselt number at the stagnation region of the blade is not really influenced for relatively high variation of flow incidence angle for the air jet experiment seems promising. As far as the tests in the turbine facility CT3 with the single-layer gauges are concerned (chapter 4), the test conditions differ. The inlet Reynolds of the second stator is around *690,000* (based on the axial chord of the stator blade, $C_{ax} = 54.9mm$) and the Nusselt number at the stagnation point has been measured with the single-layer gauge 11 equal to *4,000* (based on the blade chord, $C = 66.36mm$) (paragraph 4.5.2). Thus, the values of Reynolds number and Nusselt number based on the cylindrical diameter (*3.498mm*) are *43,900* and *211* respectively. Hence, the ratio $Nu/Re^{1/2}$ is *1.007* and it could still be independent of the flow angle for more than ±*18°* of $\Delta\Phi$ (see Figure 7-5). According to Eq. (43), the free stream turbulence is calculated equal to *1.6%*, somehow lower than its measured value, which is around *1.8%*. An equivalence between the Nusselt number and the Reynolds number values based on the diameter of the approximated cylinder and the values based on the axial chord of the second stator blade of CT3 is given in Table 7-1 for the tests in CT3 and the calibration tests.

		Axial chord 54.9mm	Diameter 3.5mm
Tests in CT3	Nu (single-layer)	3310	211
	Re	690000	43900
Calibration Tests	Nu_1 (single-layer)	1318	84
	Nu_1 (two-layer)	1365	87
	Re_1	98547	6279
	Nu_2 (single-layer)	1240	79
	Nu_2 (two-layer)	1287	82
	Re_2	84814	5404

Table 7-1: Equivalence between the non dimensional numbers based on the diameter of the approximated cylinder and the blade axial chord of CT3

The conclusion that the value of Nusselt number at the stagnation region is not really influenced for relatively high variation of flow incidence angle can be very important for a real test in the turbine facility CT3. Even if the flow angle is not exactly the design one, the experiments are expected to give a good evaluation of the Nusselt number at the stagnation region. However, this conclusion has also to be reinforced through a most accurate determination than a correlation in cylinders. As the values of Nusselt number and Reynolds number that are observed during the tests in the CT3 facility cannot be easily reproduced by an air jet nozzle, these tests are simulated by a numerically generated flow on a two dimensional blade section (paragraph 7.3). The numerical code is called TRAF2D and it is a two dimensional viscous solver for cascade predictions. Details on the code could be found in Arnone et al. (1992) and Arnone and Swanson (1993).

7.3 Numerical determination of the stagnation point for a variation of flow incidence angle

The numerical determination of the stagnation point on the blade profile used at the second stator of the turbine facility CT3 for a variation of flow incidence angle is performed with the code TRAF2D. The latter simulates the flow passing a single blade row (cascade) by solving the Navier-Stokes equation. The constant blade wall temperature as boundary condition is preferred (in stead of the adiabatic wall) to also enable Nusselt number calculations on the blade wall. The inlet boundary conditions (pressure and temperature) are uniform and the calculations are two dimensional. The y^+ along the blade wall profile is everywhere less than *0.2*.

The inlet time-averaged gas temperature and the pressure ratio across the blade of the second stator during the test in the CT3 facility combined with different flow angles are used as boundary conditions for the calculations with TRAF2D. Three of the isentropic Mach number distributions are shown in Figure 7-6 and correspond to zero $\Delta\Phi$ (which is *13°* flow design angle), to *-20°* $\Delta\Phi$ and to *+20°* $\Delta\Phi$. The results are shown as a function of the non-dimensional axial coordinate x/C_{AX} defined in Figure 4-5. The zero value of the ratio x/C_{AX} corresponds to the first point of the blade profile in the axial direction, which does not coincide with the theoretical stagnation point for $\Delta\Phi=0$; the latter is slightly further to the pressure side (lower isentropic Mach number of the black solid line in Figure 7-6). The distribution for *0* degree is the design one for the second stator blade in the CT3 facility; an overshoot is introduced at the suction side for *–20°*, because the stagnation point moves a lot towards the pressure side; for the case of *+20°*, the stagnation point moves to the suction side. This movement of the stagnation point according to the angle of the flow is also shown in Figure 7-7 with black triangles, for 9 different flow angles. On the same graph, the positions of the four gauges that are situated around the stagnation region (gauges 9, 10, 11, 12, see Figure 4-2) are indicated with red squares. The vertical axis of the graph stands for the blade profile in x/C_{AX}, where positive values correspond to the suction side and negative values to the pressure side. The horizontal axis shows the flow incidence angle. For example, for an incidence $\Delta\Phi=-5°$ (positive incidence angle, Figure 7-1), the position of the stagnation point moves to the pressure side at $x/C_{AX}=-0.018$. The gauge positions on the blade profile depend only on the value of the ratio x/C_{AX} and do not move with different $\Delta\Phi$; thus, they are placed on the graph at $\Delta\Phi=0$.

The first observation is that at design conditions ($\Delta\Phi=0$), the stagnation point is between the gauges 11 and 10, much closer to the gauge 10. Thus, higher values of Nusselt numbers during the measurements in the turbine facility CT3 are expected for gauge 11 and 10. There are five repeated measurements in CT3 for the gauges 9 and 11 (shown in Figure 7-8, with test numbers from 51 to 47) and only one measurement for the gauges 10 and 12 (test number 45). All these tests in the CT3 facility are performed for the same flow incidence angle (and they are extensively discussed in paragraph 4.5.2). On the same graph, information from Figure 7-7 is superposed: the position of four stagnation points (that correspond to $\Delta\Phi$ = *-5°, 0, 5°, 20°*) is shown with the orange vertical dotted lines.

More into detail, the Nusselt number difference between the gauges 10, 11 and 12 seems to be small, with a slightly lower value for the gauge 12. As there are no repeated tests for the gauge 10, the uncertainty on its Nusselt number value can not be determined. It is possible that five additional similar tests could give an average value higher than the test number 45 alone. In addition, the design flow incidence angle (*ΔΦ=0*) suggests that the theoretical stagnation point is closer to gauge 10 than 11. A stagnation point closer to gauge 11 would imply a very high negative incidence (*ΔΦ~15°*).

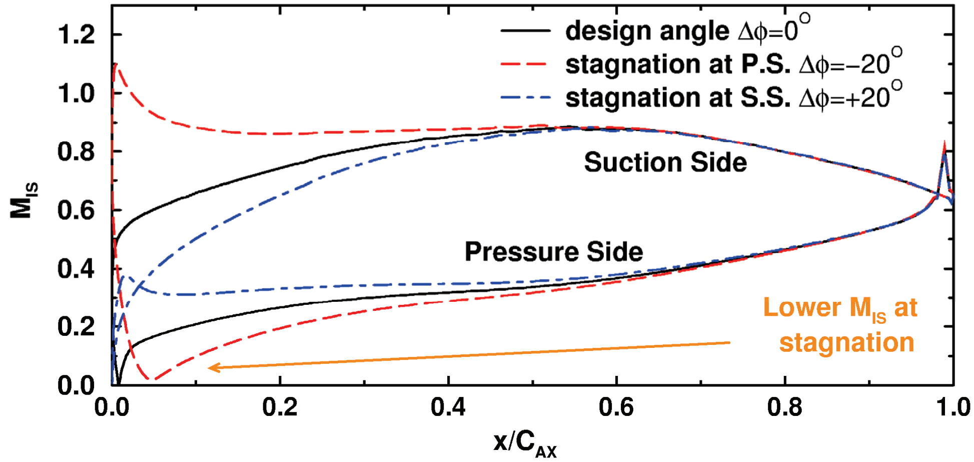

Figure 7-6: Isentropic Mach number distributions for three different flow incidence angles (TRAF2D)

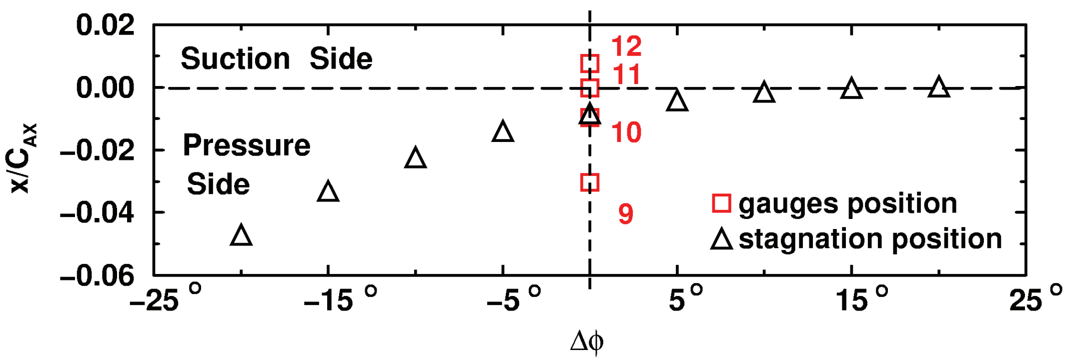

Figure 7-7: Movement of the stagnation point according to the flow incidence angle (TRAF2D)

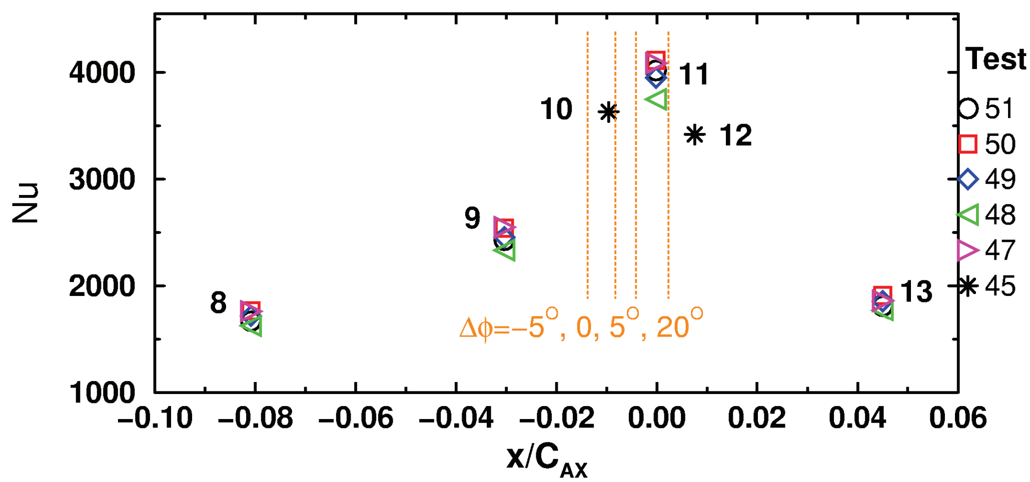

Figure 7-8: Nusselt number measurements in CT3 at the midspan of the leading edge of the second stator blade compared to the position of the stagnation point for different flow incidence angles

To investigate further the position of the stagnation point during a test in the CT3 facility, results of additional pressure measurements are shown in Figure 7-9 for the hole profile at midspan (see Figure 7-1) where gauge 10 has the highest static pressure, thus the lowest velocity and seems to be closer to the stagnation point. The fact that it is the gauge 11 that determines the highest Nusselt number in Figure 7-8 could eventually be explained from the limitation of the data reduction program to take into account curvature effects (paragraph 3.6). Note that the radius of the blade is much smaller at the position of the gauge 11 than at the position of the gauge 10. In chapter 6, where the influence of the curvature on the Nusselt number calculations is discussed, it seems that the Nusselt number values of gauges 11 and 10 can be considered equal (see Figure 6-3).

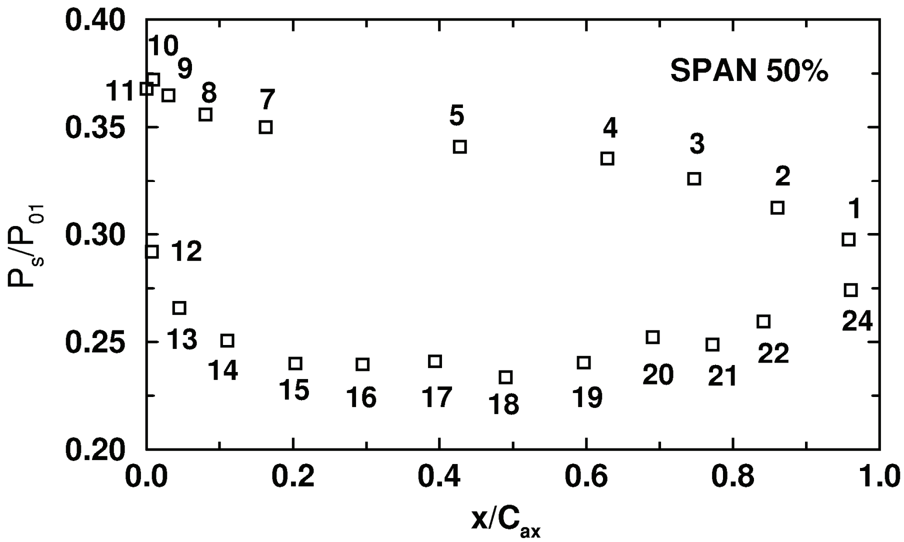

Figure 7-9: Pressure measurements in CT3 at the midspan of the leading edge of the second stator blade (Paniagua et al, 2003)

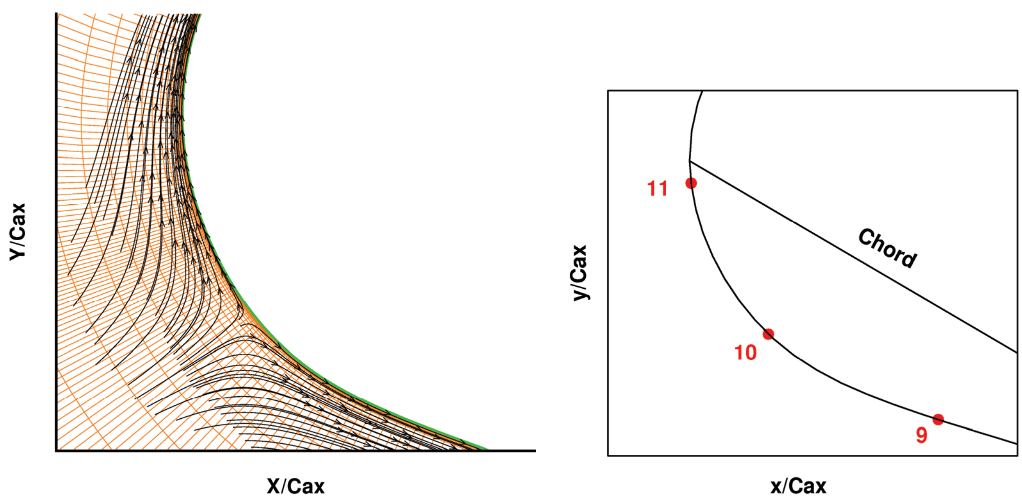

Figure 7-10: two dimensional representation of the flow, calculated with TRAF2D, at the leading edge at midspan of the second stator blade (left) compared to the position of the gauges (right)

In order to reinforce the conclusion that the calculated stagnation point is very close to gauge 10 for the design flow incidence angle, a two dimensional representation of the flow, calculated with TRAF2D, at the leading edge at midspan of the second stator blade (left graph) compared to the position of the gauges (right graph) is shown in Figure 7-10.

A last observation based on the above analysis is that the stagnation point moves considerably with the flow angle, mainly at the pressure side of the blade for positive incidence ($\Delta\Phi<0$). A closer look at the geometry of the leading edge of the blade could justify this following observation. The suction side is more curved and better approximated to a cylinder, contrary to the pressure side that the blade profile curvature gets very small at the position of gauge 9 (see Figure 4-2).

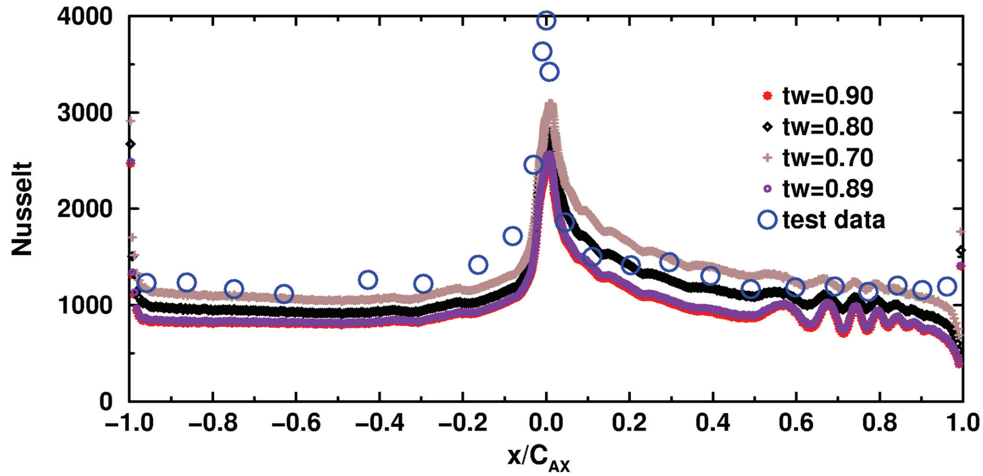

Figure 7-11: Nusselt number calculation at midspan of the second stator blade (TRAF2D)

Last, TRAF2D is used for Nusselt number calculations at midspan of the second stator blade (Figure 7-11). The solution is given under a constant wall temperature boundary condition for different ratios of wall temperature to total gas temperature at the inlet of the blade (t_W parameter). The calculations with different choices of the value of the ratio t_W are performed in order to demonstrate the sensitivity of the Nusselt number calculations from the gas to wall changes and seems to be not negligible compared to its average value. The case of $t_W = 0.89$ corresponds to the measured values during a test in the turbine facility CT3; while for the same flow conditions, the actual measured Nusselt number by the gauges is indicated with circles. The Nusselt number, which is based on the blade chord (*66.36mm*) is considerably underestimated in the stagnation region of the blade at midspan, although a fully turbulent boundary layer is used for the Nusselt number determination. The program uses the Baldwin-Lomax turbulence model (Baldwin and Lomax, 1978), which is fast in calculations but not as accurate as the k-ε or k-ω models. The free stream turbulence intensity is not used for the prediction of the Nusselt number, although it is a parameter very important for the Nusselt number levels, especially at the leading edge of the blade. In addition, the main difference between the code results and the measurements is that the code assumes uniform inlet flow to the blade, contrary to the reality where the rotor blade wakes generate high free stream turbulence.

7.4 References

Arnone A., Swanson R.C., 1993, *'A Navier-Stokes Solver for Turbomachinery Applications'*, J. of Turbomachinery, vol. 115(2), pp 305-313

Arnone A., Liou, M-S, Povinelli, L.A., 1992, *'Navier-Stokes Solution of Transonic Cascade Flow Using Non-Periodic C-type Grids'* J. of Propulsion and Power, vol. 8(2), pp 410-417

Baldwin B.S., Lomax H., 1978, *'Thin Layer Approximation and Algebraic Modelfor Separated Turbulent Flows'*, AIAA 16th Aerospace Sciences Meeting, paper 78-257

Kestin J., Wood R., 1971, *'The influence of turbulence on mass transfer from cylinders'*, J. of Heat Transfer, vol. 93C, pp 321-327

Paniagua G., Billiard, N., Denos R., Sieverding C.H., 2003, *'Interference and clocking effects in a one and a half stage turbine: Time-Averaged Endwall Pressure Measurements'*, Technical Report No B4/VKI/2/1